Hybrid optoacoustic and ultrasound imaging in three dimensions and real time by optical excitation of a passive element

Thomas Felix Fehm[1,2] Xosé Luís Deán-Ben[1] and Daniel Razansky[1,2]

[1]Institute for Biological and Medical Imaging (IBMI), Helmholtz Zentrum München, Neuherberg, Germany, [2]Faculty of Medicine, Technische Universität München, Munich, Germany

ABSTRACT

Pulse-echo ultrasound and optoacoustic imaging possess very different yet highly complementary advantages of mechanical and optical contrast in living tissues. Integration of pulse-echo ultrasound with optoacoustic imaging may therefore significantly enhance the potential range of clinical applications. Nonetheless, efficient integration of these modalities remains challenging owing to the fundamental differences in the underlying physical contrast, optimal signal acquisition and image reconstruction approaches. We report on a new method for hybrid three-dimensional optoacoustic and pulse-echo ultrasound imaging based on passive generation of ultrasound with a spherical optical absorber, thus avoiding the hardware complexity of active ultrasound generation. The proposed approach allows for acquisition of complete hybrid datasets with a single laser interrogation pulse, resulting in simultaneous rendering of ultrasound and optoacoustic images at a rate of 10 volumetric frames per second. Real time image rendering for both modalities is enabled by using parallel GPU-based implementation of the reconstruction algorithms. Performance is first characterized in tubing phantoms followed by in-vivo measurements in healthy human volunteers, confirming general clinical applicability of the method.

Keywords: optoacoustic, ultrasonography, medical image reconstruction, acoustic scattering

1. INTRODUCTION

Pulse-echo ultrasound (US) is the most prominent imaging tool applied in modern clinical diagnostics. It is used in several fields from obstetrics and gynecology to cancer staging, intravascular and cardiac diagnostics[1, 2]. Its specificity and diagnostic value however is limited since the contrast correlates with the amount of acoustic mismatch and therefore mainly reveals structural information[3]. Integration of US with optoacoustic (OA) imaging may therefore significantly enhance the potential range of applications by bringing the optical contrast advantages of the optoacoustic modality such as spectral specificity[4, 5] and functional hemodynamic contrast[6].

Several two-dimensional (cross-sectional) imaging approaches have been previously investigated for combining OA with US. Commonly, the traditional US linear array is combined with a fiber-guided light irradiation on one or both sides of the array[7] and pulse-echo ultrasound and optoacoustic signals are recorded in an alternate order. An alternative approach for producing laser-induced US to interrogate the object in a conventional cross-sectional optoacoustic scanner consisting in introducing strong absorbers positioned outside the object in the path of the excitation light[8]. In this way, ultrasound transmission parameters like the speed of sound distribution and attenuation maps can be extracted along with the optoacoustic absorption maps. However, as opposed to the relatively narrowband back-reflected US radiation, optoacoustically-generated signals usually have an ultra wide bandwidth and manifold higher tissue contrast. The application of acoustic focusing and common US beamforming or synthetic aperture approaches for OA image rendering is then generally challenging, leading to poor imaging performance for techniques based on these reconstruction approaches[9]. In this letter, we introduce a new concept for combined three-dimensional ultrasound and optoacoustic imaging with an acoustic beam excited via transient absorption of the excitation light. The optoacoustically-induced signals from the imaged tissues are then simultaneously recorded with the later arriving back-scattered ultrasonic waves by means of the spherical matrix array transducer. In this way, we are able to reproduce three-dimensional optoacoustic and pulse-echo ultrasound images in real time.

Photons Plus Ultrasound: Imaging and Sensing 2015, edited by Alexander A. Oraevsky, Lihong V. Wang
Proc. of SPIE Vol. 9323, 93232X · © 2015 SPIE · CCC code: 1605-7422/15/$18
doi: 10.1117/12.2080138

Downloaded From: http://proceedings.spiedigitallibrary.org/ on 04/21/2016 Terms of Use: http://spiedigitallibrary.org/ss/TermsOfUse.aspx

2. METHODS

2.1 EXPERIMENTAL SETUP

The proposed hand-held implementation for hybrid optoacoustic and ultrasound imaging as introduced earlier[10] is depicted in Figure 1. The ultrasound beam is excited by light absorption at a passive element (PE) comprising a highly absorbing carbon microsphere with an approximate diameter of 400 µm (SPI-Supplies) located between the sample and the detection array. A spherically-shaped array consisting of 256 piezocomposite elements[11] (Imasonic SaS, Voray, France) is employed to detect the back-scattered ultrasound signals. The individual detection elements have a size of 3x3 mm^2, a central frequency of 4 MHz and a -6 dB bandwidth of 100%. A central cavity is included in the array to enable coaxial optical excitation. In order to guarantee efficient illumination, the passive absorbing element was embedded in agar and placed along the central axis of the array. Nanosecond-duration light pulses for optoacoustic excitation are generated by a tunable optical parametric oscillator (wavelength range ~690-900 nm) laser source (SpitLight, Innolas Laser GmbH, Krailling, Germany) at a pulse repetition frequency (PRF) of 10 Hz. The beam is then guided through a custom-made fiber bundle (CeramOptec GmbH, Bonn, Germany) that provides a Gaussian illumination profile at the tissue surface with a full-width at half maximum (FWHM) of approximately 10 mm. The time-resolved pressure signals of the 256 detectors are simultaneously digitized by a custom-made high-speed data acquisition system (Falkenstein Mikrosysteme GmbH, Taufkirchen, Germany) and triggered with the Q-switch output of the laser. The position of the carbon microsphere allows separating the optoacoustic waves generated within the tissue and the echoes from the passive-element ultrasound beam by simple time-windowing of the collected signals.

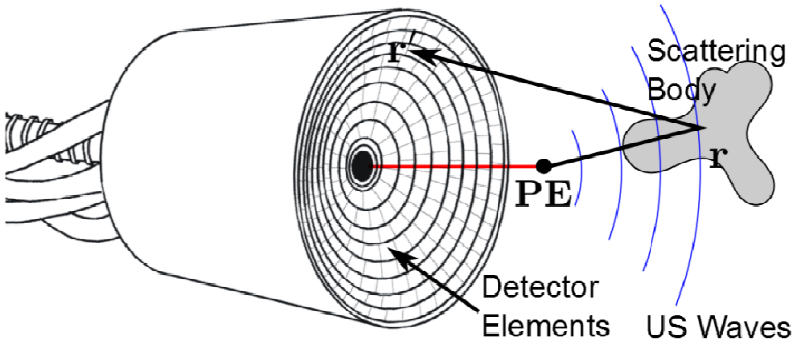

Figure 1. Hand-held probe with the passive element (PE). The PE is excited by laser light delivered from a fiber cable placed in the middle of the detector. The excited acoustic wave then becomes scattered before they are detected by the spherical array.

2.2 THEORY AND IMAGE RECONSTRUCTION

Three-dimensional optoacoustic image reconstruction is performed by implementing a back-projection formula[12]. The optoacoustic amplitude in arbitrary units at a given pixel $H(r'_j)$ is given by

$$H(r'_j) \approx \sum_i p_f(r_i, t_{ij}) - t_{ij} \frac{p_f(r_i, t_{ij})}{\partial t}, \quad (1)$$

being r_i the position of the *i*-th transducer element and $t_{ij} = |r'_j - r_i|/c$ the time-of-flight between r'_j and r_i, further assuming a constant speed of sound c in the medium. $p_f(r_i, t_{ij})$ represents the optoacoustically-induced spatio-temporal pressure distribution, obtained by measuring the signals around the object. For accurate signal recovery and optimal noise damping, a filter combining deconvolution with the impulse response of the elements, differentiation and a band-pass filter with cut-off frequencies of 0.75 and 7 MHz was applied to all recorded signals in the time domain.

A similar reconstruction framework can in principle be considered for reconstructing the distribution of acoustic scatterers within the region of interest. However, several issues must be taken in consideration. The frequency spectrum of the signal emitted from the PE depends on its size, density, the longitudinal and transversal speed of sound[13]. The temporal profile of the optoacoustic signal emitted by the particular PE used in this study was measured using a

Downloaded From: http://proceedings.spiedigitallibrary.org/ on 04/21/2016 Terms of Use: http://spiedigitallibrary.org/ss/TermsOfUse.aspx

calibrated broadband hydrophone (Precision Acoustics Ltd., Dorset, UK) and is shown in Fig. 2(a) along with its spectrum (Fig. 2(b)). The signal of the PE was low-pass filtered at 6 MHz to remove high frequency noise. Clearly, the emitted spectrum is significantly broader than the effective detection bandwidth of the transducer elements. On the other hand, the directivity and frequency spectrum of the back-scattered pressure waves is affected by the type of scattering event. For instance, Rayleigh scattering would yield an isotropic far-field pattern and a frequency dependence of the scattering cross-section given by $1/\lambda^4$, where λ is the acoustic wavelength[14]. Under the common assumption of single scattering events in soft biological tissues (weak scattering), the spatial distribution of scatterers can be reconstructed by means of a back-projection approach similar to the optoacoustic case. Specifically, the ultrasound image at a certain voxel $U(r'_j)$ is estimated as

$$U(r'_j) = \sum_i s(r_i, t_{hij}), \tag{2}$$

being $t_{hij} = |r_h - r'_j|/c + |r'_j - r_i|/c$ the total time of flight from the location of the passive element r_h to the location of the acoustic scatterer r_j and from there to the location of the detector r_i. In deriving an efficient implementation of reflection-mode ultrasound imaging using optoacoustically-induced radiation in the PE, $s(r_i, t_{hij})$ in Eq. (2) was taken as the filtered pressure $p_f(r_i, t_{ij})$, whereas a band-pass filter was applied (cut-off frequencies set between 2Mhz and 4Mhz) in order to optimize resolution and contrast of the images. In this way, the lower frequency boundary of the detected spectrum is responsible for establishing the diffraction-limited spatial resolution in the US imaging mode. Similarly to the conventional pulse-echo ultrasonography[15], it is assumed here that the size of acoustic scatterers in the imaged tissue is much smaller than the wavelength of the detected waves.
Visualization in both optoacoustic and ultrasound modes relies on a GeForce GTX 780 implementation of the reconstruction algorithms using CUDA.

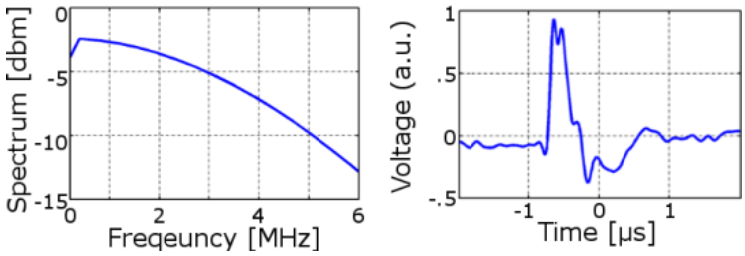

Figure 2. Power spectrum density of the pressure wave emitted by the PE absorber (left) and temporal profile of the recorded signal (right).

2.3 PHANTOM EXPERIMENTS

The suggested hybrid approach was tested by phantom experiments. A knot was tangled using a polyethylene tube with an inner diameter of 0.6 mm (Fig 3(c)) and was positioned around the center of the spherical ultrasound array, to ensure maximum sensitivity of all elements. The wavelength of the laser was set to 750 nm. Injection of different scattering and absorbing substances into the tubing was performed using an automatic injection pump (Harvard Apparatus, Holliston, USA) using a volume rate of 0.028 ml/s (~1cm/s). For real-time visualization of dynamic phenomena, two injection experiments were performed. In the first experiment, the tubing initially contained air, which was slowly replaced by the ink solution, having effective optical absorption coefficient of μ_a=2.3 cm^{-1}. The injection rate was maintained constant until the phantom was completely filled with the ink solution. In the second experiment, the tube was initially filled with the ink solution while the microbubble contrast agent (SonoVue®, Bracco Group, Italy) was subsequently injected for contrast enhancement. Results of the imaging experiments are presented in Fig. 3, clearly evincing that the spatial distribution dynamics of both light absorption and acoustic scattering can be simultaneously imaged in real time. Three representative time instants are shown in Fig. 3 for the two imaging experiments. While air and ink only provide strong contrast in ultrasound or optoacoustic images, respectively, the microbubble solution generates significant contrast for both modalities. To this end, microbubble contrast agents have significantly enhanced the imaging capacities in medical ultrasound diagnosis, drug and gene delivery applications[16]. Here it was found that the common ultrasound contrast agent also provides detectable contrast for optoacoustic imaging at clinically applied concentration. The shape of the knot can be clearly distinguished in all images while the interface between the substances inside the tubing can be further

Downloaded From: http://proceedings.spiedigitallibrary.org/ on 04/21/2016 Terms of Use: http://spiedigitallibrary.org/ss/TermsOfUse.aspx

tracked in real time, as shown e.g. in Fig. 3(a) for t=0.7s (labelled B). An additional example of well-registered OA and US images can be seen in Fig. 2a for t=0s, where an ink droplet leftover from a previous experiment (labelled A) can be clearly identified inside the tubing. On the other hand, the onset of the ultrasound signal in Fig. 2b is delayed and reaches its full strength when the tubing is completely filled with the ultrasound contrast agent. The maximum value of the ultrasound image in Fig. 3(b) at t=1.5s was found to be approximately two thirds of the air filled phantom in Fig. 3(a) at t=0s.

A second set of experiments was carried out in order to provide an estimate of the lateral resolution and size of the field of view for the back-scattering ultrasound mode. A glass microsphere with an approximate diameter of 500 µm (Cospheric, Santa Barbara, USA) was positioned in the vertical plane corresponding to the center of the spherical probe. The reflected signals where then recorded for different lateral positions of the sphere and the ultrasound images were reconstructed using Eq. (2). The size of the reconstructed glass microsphere for each individual image was defined as the FWHM. Analogously, the field of view was defined as the FWHM of the maximum pixel value as a function of the lateral position of the microsphere. This results in an estimated lateral size of the field of view of 10 mm. On the other hand, the size of the reconstructed sphere was approximately 500 µm for all lateral positions, indicating that the spatial resolution in the pulse-echo ultrasound mode is better than 500 µm. Clearly, the size of the reconstructed sphere is affected by the diameters of both the light absorber and the acoustic scatterer so that a better estimate of the resolution is achieved when using smaller microspheres, which was however not accomplished in the current study due to rapid deterioration of the contrast to noise ratio for smaller scatterers. Nevertheless, it was previously shown that the resolution of the optoacoustic images, achieved by the spherical matrix array used in this study, was in the range 200 µm at the geometrical center of the sphere[11] so that a similar resolution would also be expected for the ultrasound mode.

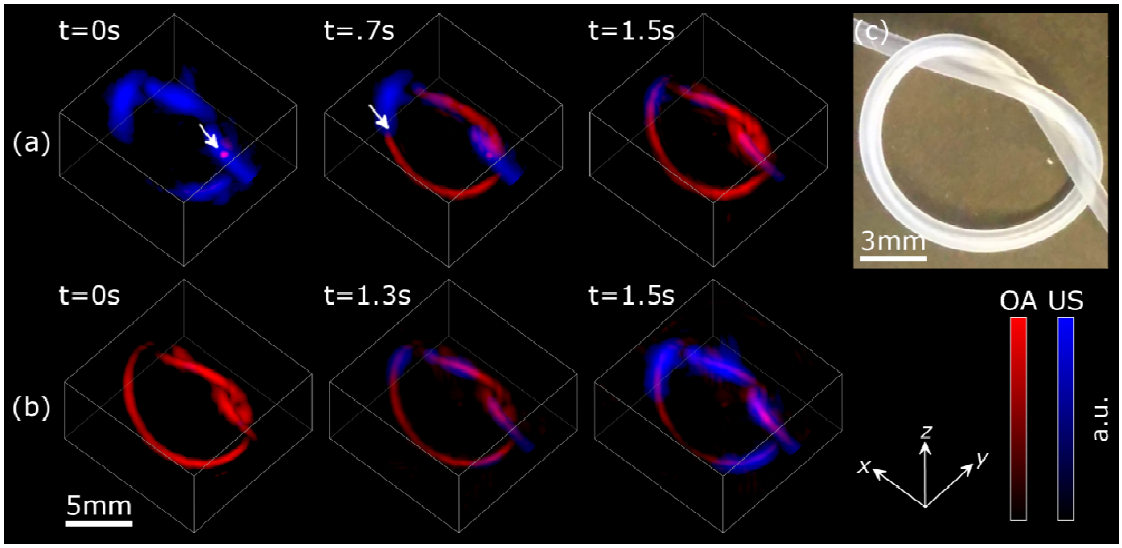

Figure 3. Three-dimensional hybrid visualizations of fast contrast variations at video rate. (a) The reconstructed optoacoustic (OA) and ultrasound (US) images represent the experiment corresponding to the tubing phantom filled with air before an ink solution (μ_a=2.3 cm-1) is injected at t=0. Details like an ink droplet leftover from a previous experiment and the boundary between air and the ink solution when the tubing is partially filled are indicated by white arrows. (b) Results from the second experiment where the phantom is initially filled with the ink solution before the microbubble contrast agent is injected. The maximum ultrasound signal strength provided by the microbubbles is achieved at t=1.5s.

2.4 HUMAN FINGER EXPERIMENT

The performance of the hybrid probe in imaging of living biological tissues was showcased in a finger of a healthy volunteer. Human experiments were performed in full accordance with work safety regulations of Helmholtz Center Munich. A representative hybrid contrast image is displayed in Fig. 4. Clearly, while the ultrasound signals mainly manifest features related to the acoustic back-scattering at the surface of the skin and the bone (labeled on blue color scale in Fig. 4(a)), the optoacoustic data emphasizes a different type of optical absorption contrast arising from blood vessels located between the skin and the bone (labeled on red color scale). The additional structural contrast provided by superimposition of the US images may facilitate localization of the functional blood contrast visualized in the optoacoustic mode. Furthermore, the position of structures like the skin or the bone represent a valuable prior imaging

Downloaded From: http://proceedings.spiedigitallibrary.org/ on 04/21/2016 Terms of Use: http://spiedigitallibrary.org/ss/TermsOfUse.aspx

information that can be subsequently employed to determine areas with a different speed of sound or regions where strong acoustic scattering takes place, thus helping to improve the optoacoustic reconstructions[17, 18].

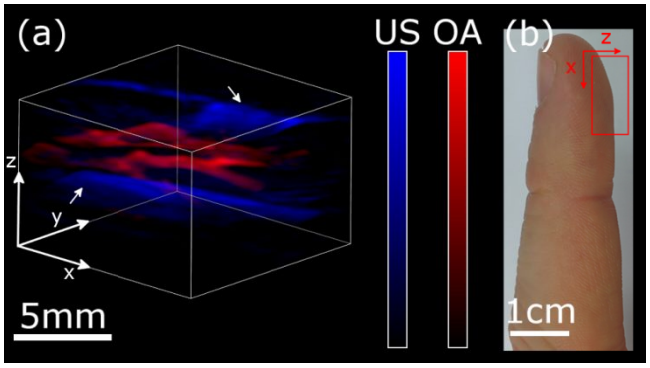

Figure 4. Hybrid imaging of finger in a healthy volunteer. (a) Three dimensional views of the optoacoustic (OA) and ultrasound (US) reconstructions. The ultrasound image allows visualizing the location of the skin and the bone surface (labelled by white arrows) while optoacoustic signals mainly convey contrast of the blood vessels. The imaged region in the finger is shown in (b).

3. RESULTS AND DISCUSSION

Several limitations of the newly introduced approach require further attention. The three-dimensional matrix array probe, employed in the current study, is specifically optimized for optoacoustic tomographic imaging in a hand-held mode. However, its relatively low number of piezoelectric elements, their orientation and the large pitch are not optimal for the delay-and-sum beamforming approach used in standard pulse-echo ultrasound imaging, which may result in significant grating lobe artifacts and loss of spatial resolution and contrast[19]. On the other hand, it is also important to notice that the conventional three-dimensional ultrasound, performed in the active send-receive mode, is severely limited in terms of its time resolution due to the large number of A-lines to be scanned[20]. Here we have demonstrated ultrasound image acquisition at an unprecedented volumetric frame rate of up to 10 Hz but significantly better time resolution can be achieved by employing lasers with higher pulse repetition frequency. A better hardware design, particularly pertaining the size, shape and position of the passive element(s), is yet another crucial aspect for achieving the optimum amplitude and frequency content of the ultrasound beam and hence maximize image contrast and resolution. Finally, a finer design of the matrix detection array may further contribute to improving image quality in both optoacoustic and ultrasound modes.

In conclusion, the capacity of hybrid ultrasound and optoacoustic imaging in three dimensions and real time has been showcased for the first time. As opposed to possible other techniques requiring active excitation of ultrasound, no significant hardware complexity was added beyond the original optoacoustic imaging probe design. Overall, the demonstrated volumetric imaging speed and the synergetic combination of optoacoustics and ultrasound anticipate emergence of powerful new applications around the newly introduced approach.

4. REFERENCES

[1] P.W. Callen, Ultrasonography in obstetrics and gynecology, Elsevier Health Sciences, 2011.

[2] M. Castillo, J.R. Wienke, Ultrasonography in Vascular Diseases: A Practical Approach to Clinical Problems, Academic Radiology, 9 (2002) 838.

[3] G. Schmidt, Differential Diagnosis in Ultrasound Imaging: a Teaching Atlas, Thieme, 2011.

[4] L.V. Wang, S. Hu, Photoacoustic Tomography: In Vivo Imaging from Organelles to Organs, Science, 335 (2012) 1458-1462.

[5] X.L. Deán-Ben, D. Razansky, Adding fifth dimension to optoacoustic imaging: volumetric time-resolved spectrally enriched tomography, Light: Science & Applications, 3 (2014) e137.

[6] X. Wang, Y. Pang, G. Ku, X. Xie, G. Stoica, L.V. Wang, Noninvasive laser-induced photoacoustic tomography for structural and functional in vivo imaging of the brain, Nature biotechnology, 21 (2003) 803-806.

[7] J.J. Niederhauser, M. Jaeger, R. Lemor, P. Weber, M. Frenz, Combined ultrasound and optoacoustic system for real-time high-contrast vascular imaging in vivo, Medical Imaging, IEEE Transactions on, 24 (2005) 436-440.

Downloaded From: http://proceedings.spiedigitallibrary.org/ on 04/21/2016 Terms of Use: http://spiedigitallibrary.org/ss/TermsOfUse.aspx

[8] J. Jose, R.G. Willemink, W. Steenbergen, C.H. Slump, T.G. Leeuwen, S. Manohar, Speed-of-sound compensated photoacoustic tomography for accurate imaging, Medical Physics, 39 (2012) 7262.
[9] C. Kim, T.N. Erpelding, L. Jankovic, M.D. Pashley, L.V. Wang, Deeply penetrating in vivo photoacoustic imaging using a clinical ultrasound array system, Biomedical optics express, 1 (2010) 278-284.
[10] T.F. Fehm, X.L. Deán-Ben, D. Razansky, Four dimensional hybrid ultrasound and optoacoustic imaging via passive element optical excitation in a hand-held probe, Applied Physics Letters, 105 (2014) 173505.
[11] X.L. Deán-Ben, D. Razansky, Portable spherical array probe for volumetric real-time optoacoustic imaging at centimeter-scale depths, Optics Express, 21 (2013) 28062-28071.
[12] M. Xu, L. Wang, Universal back-projection algorithm for photoacoustic computed tomography, Physical Review E, 71 (2005).
[13] M. Khan, G. Diebold, The photoacoustic effect generated by an isotropic solid sphere, Ultrasonics, 33 (1995) 265-269.
[14] J.J. Bowman, T.B.A. Senior, P.L.E. Uslenghi, J.S. Asvestas, Electromagnetic and acoustic scattering by simple shapes, Rev. print. ed., Hemisphere Pub. Corp., New York, 1987.
[15] K.K. Shung, G.A. Thieme, Ultrasonic scattering in biological tissues, CRC Press, 1992.
[16] E. Stride, N. Saffari, Microbubble ultrasound contrast agents: a review, Proceedings of the Institution of Mechanical Engineers, Part H: Journal of Engineering in Medicine, 217 (2003) 429-447.
[17] J. Jose, R. Willemink, S. Resink, D. Piras, Passive element enriched photoacoustic computed tomography (PER PACT) for simultaneous imaging of acoustic propagation properties and light absorption, Optics, (2011).
[18] X.L. Dean-Ben, V. Ntziachristos, D. Razansky, Acceleration of Optoacoustic Model-Based Reconstruction Using Angular Image Discretization, IEEE Transactions on Medical Imaging, 31 (2012) 1154-1162.
[19] K.E. Thomenius, Evolution of ultrasound beamformers, in: Ultrasonics Symposium, 1996. Proceedings., 1996 IEEE, IEEE, 1996, pp. 1615-1622.
[20] A. Ng, J. Swanevelder, Resolution in ultrasound imaging, Continuing Education in Anaesthesia, Critical Care & Pain, 11 (2011) 186-192.

Downloaded From: http://proceedings.spiedigitallibrary.org/ on 04/21/2016 Terms of Use: http://spiedigitallibrary.org/ss/TermsOfUse.aspx